Direct observation of lithium-ion transport under an electrical field in Li_xCoO_2 nanograins

Xiaojian Zhu[1,2], Chin Shen Ong[3], Xiaoxiong Xu[1,2], Benlin Hu[1,2], Jie Shang[1,2], Huali Yang[1,2], Sadhana Katlakunta[1,2], Yiwei Liu[1,2], Xinxin Chen[1,2], Liang Pan[1,2], Jun Ding[1,3] & Run-Wei Li[1,2]

[1]Key Laboratory of Magnetic Materials and Devices, Ningbo Institute of Materials Technology and Engineering (NIMTE), Chinese Academy of Sciences (CAS), Zhejiang, Ningbo 315201, People's Republic of China, [2]Zhejiang Province Key Laboratory of Magnetic Materials and Application Technology, Ningbo Institute of Materials Technology and Engineering (NIMTE), Chinese Academy of Sciences (CAS), Zhejiang, Ningbo 315201, People's Republic of China, [3]Department of Materials Science and Engineering, National University of Singapore 119260, Singapore.

The past decades have witnessed the development of many technologies based on nanoionics, especially lithium-ion batteries (LIBs). Now there is an urgent need for developing LIBs with good high-rate capability and high power. LIBs with nanostructured electrodes show great potentials for achieving such goals. However, the nature of Li-ion transport behaviors within the nanostructured electrodes is not well clarified yet. Here, Li-ion transport behaviors in Li_xCoO_2 nanograins are investigated by employing conductive atomic force microscopy (C-AFM) technique to study the local Li-ion diffusion induced conductance change behaviors with a spatial resolution of ∼10 nm. It is found that grain boundary has a low Li-ion diffusion energy barrier and provides a fast Li-ion diffusion pathway, which is also confirmed by our first principles calculation. This information provides important guidelines for designing high performance LIBs from a point view of optimizing the electrode material microstructures and the development of nanoionics.

N anoionics mainly covers a variety of modern technologies including energy conversion and storage, information storage and other technologies related to electrochemical reactions at a nano-scale[1–6]. Different from nanoelectronics, nanoionics is focused on the study of ion transportation and has attracted great attentions in the past decades. A typical example is Lithium-ion batteries (LIBs) which have already found their widely applications in portable electronic device as power sources[3,7]. To achieve rechargeable LIBs that could meet the urgent demands from high power devices, many technical challenges, such as good high-rate capability and large discharge capacity, need to be overcome[3,7]. It is reported that nanostructured electrodes, i.e. grains in the nano-size range, offering distinct metrics including a short ion and electron transport length and a large surface area, are beneficial to improve LIBs' performances[8,9]. Unfortunately, so far, the behaviors of Li-ion transport within the electrodes composed of nano-sized grains at a nano-scale are not well understood, and some crucial information like the location of the fast diffusion paths, kinetics of Li-ion in the grains and at the internal grain interfaces is virtually unknown. This can be partially attributed to the lack of suitable and efficient characterization techniques for clarifying the mechanisms involved in LIBs operation processes at a nano-scale[10], which hinders us to understand the interrelationship between the electrode microstructure and battery performances[11,12].

Until now, several techniques have been used to investigate Li-ion transportation, including scanning electron microscopy, scanning probe microscopy based techniques, magnetic resonance imaging method and especially high resolution transmission electron microscopy[13–23]. These methods have already provided very important information about the LIBs working mechanisms which guide us to develop LIBs with improved performances. However, some of these methods suffer from at least one of several disadvantages, for example, inconvenient sample preparation, high environmental sensitivity, non-quantitative measurement and especially limited spatial resolution, respectively. Therefore, some new techniques that can further provide insights into Li-ion diffusion at a nano-scale with a high spatial resolution and (semi-)quantitative measurement capability, are highly desired.

As one of the most widely used cathode materials, $LiCoO_2$ is very suitable for a typical model material to investigate Li-ion diffusion owing to its excellent stability. As reported previously, the diffusion of Li-ion can

result in Li deficiency in $LiCoO_2$ with a chemical formula of Li_xCoO_2 ($0<x<1$) and lead to a change in conductivity correspondingly[14,24,25]. Recently, Li_xCoO_2 material was proposed as one promising candidate for ionic memory[26] due to the observation of conductance change (or say resistive switching) behaviors in Li_xCoO_2 thin film, which were considered to be related with Li-ion diffusion and a change of Li content[27]. This indicates that by studying the local conductance variations under an electrical field, one may reveal the process and mechanism of Li-ion diffusion in Li_xCoO_2 material. Conductive atomic force microscopy (C-AFM) is a powerful tool that can be used to *in situ* study the local electrical transport properties of materials under a bias voltage with a spatial resolution of ~10 nm. With locating the conductive tip at the material surface, local current-voltage (I–V) characteristics can be studied *in situ*. Particularly, it also has a current resolution of ~10 pA, offering a unique opportunity for quantitative measurements.

In this work, C-AFM technique is adopted to observe electric current images of Li_xCoO_2 thin films under electrical fields. It is found that the local conductance is closely associated with the localized Li deficiency. We show that Li_xCoO_2 grain boundary area has a lower Li-ion diffusion energy barrier and higher Li-ion diffusion rate than grain interiors, which is consistent with our first principles calculation. Our findings suggest that from the point view of Li-ion diffusion behaviors, high-rate charge LIBs with a high capacity may be realized by adapting Li_xCoO_2 electrodes composed of nanograins with a large grain boundary area.

Results

Polycrystalline Li_xCoO_2 films with a thickness of ~120 nm were deposited on Pt substrates by pulsed laser deposition (PLD) method. The detailed fabrication process was reported elsewhere[28]. X-ray diffraction (XRD) pattern (see Fig. S1 in Supplementary Information) indicates a strongly preferred (003) orientation, suggesting that the Li layers are separated alternatively by CoO_2 octahedrons layers parallel to the substrate (Fig. 1a)[29].

We first characterized the conductance change behaviors in the Li_xCoO_2 thin film at a macroscopic scale (see Sample preparation in Methods). The device structure and I–V characteristics of the Pt/Li_xCoO_2/Pt stack were illustrated in Fig. 1a and b, respectively. The I–V curve showed that the Pt/Li_xCoO_2/Pt stack was of a low conductance in its pristine state. The current increased slowly with the bias voltage, and jumped abruptly, at a threshold voltage in the range of 1.5–2.0 V, to the pre-set current limit of 0.05 A which was set to protect the device from a permanent dielectric breakdown[4]. In other words, the device was switched to a high conductive state. Under negative bias voltages, the device can be switched back to a low conductive state. It is noted that at around −0.5 V, a drastic drop of current is observed. This can be understood based on the thermal-assisted conductance change process due to the large Joule-heat effect under a high current[30–32]. Notably, it is found that a higher bias voltage, 2.5 V or beyond, may damage the device without a current limitation in our case. The conductance change phenomena were well consistent with that reported in ref. 27, and the behaviors were attributed to the Li-ion diffusion under the electrical fields. The conductance ratio between the high and low conductive states in our device located in the range of three to five orders of magnitude, well consistent with the conductivity changes due to tens of percents Li content variations in Li_xCoO_2 bulk sample[25,27]. As is well-known, Li-rich Li_xCoO_2 shows a semiconductive behavior, while Li-deficient Li_xCoO_2 has a metallic conduction characteristic[25,33]. Due to the nonvolatile characteristics of the Pt/Li_xCoO_2/Pt device at both the high and low conductive states, the device resistance values at various temperatures were obtained by detecting the currents under a small voltage (*e.g.* 0.1 V). Our Pt/Li_xCoO_2/Pt stack showed a semiconductive behavior at the low conductive state, while a metallic behavior at the high conductive state (see Fig. S2), implying that the Li_xCoO_2

thin film at the high conductive state is highly Li-depleted due to the applied electrical field.

In order to investigate Li-ion diffusion at a nano-scale, C-AFM measurements were carried out to observe the local conductance change behaviors with the application of various bias voltages in the Li_xCoO_2 thin film. The Pt/Ir conductive tip was grounded in the schematic of the setup for C-AFM measurements as shown in Fig. 1c. With the tip contacted on the film and applying an appropriate bias voltage on the bottom Pt electrode, Li-ion can diffuse in the Li_xCoO_2 thin film and correspondingly cause a local change in the Li content[14,27]. Fig. 1d and e showed the morphology of the Li_xCoO_2 thin film and the corresponding current images under various electrical biases. Current images were recorded in a sequence of $0.5 \rightarrow 2.0 \rightarrow -1.5 \rightarrow -0.5$ V with a step of 0.5 V. No obvious current contrast was observed under 0.5 V at first. At 1.5 V, some bright regions corresponding to the conductive locations were detected. With further increasing the bias voltage to 2.0 V, the conductive area increased and most of the conductive regime reached the self-set compliance current level (~12 nA). While gradually reducing the bias voltage to 0.5 V, some conductive regions were reserved. These conductive regions were gradually removed under negative bias voltages and disappeared eventually at −1.5 V. An individual grain was characterized at various bias voltages and the results are shown in Fig. S3. The mean current densities ($\bar{I}$) were extracted from the current images, and the corresponding $\bar{I}$–V loop was plotted in Fig. S4 which was similar to the I–V curve in Fig. 1b. Therefore, the local bright regions in the current images can be considered to correspond to the conductive Li-deficient locations and it is feasible to employ the C-AFM technique to study the Li-ion diffusion in Li_xCoO_2 thin film at a nano-scale.

As shown in Fig. 1e, the Li-ion transport location (high conductive regions) is dependent on grain size. For example, under a bias voltage of 2.0 V, well conductive characters can be observed over the whole grain area in relative small grains, *e.g.* G1, however, for the large grains, *e.g.* G2, the grain interiors were much less conductive than grain boundary areas.

In order to investigate the differences of conductance change behaviors between the grain interiors and boundary areas, the conductance characteristics in two grains with different sizes (G3 and G4 as illustrated in Fig. 2a) were studied by I–V measurements with locating the C-AFM tip at the interiors and grain boundary areas, respectively. As shown in Fig. 2b, both G3 and G4 show similar conductance change behaviors, except that the threshold voltage for the large grain G4 is larger than that for the small grain G3. On the other hand, with locating the C-AFM tip at places near grain boundaries, the threshold voltage amplitude doesn't vary much, regardless of the grain size (not shown). The threshold voltage can reflect the Li-ion diffusion energy barrier at the location. Briefly speaking, our results indicate that the Li-ion diffusion energy barrier is closely dependent on the location in a Li_xCoO_2 grain.

We further measured the threshold voltages at different locations on a Li_xCoO_2 grain in detail. Fig. 2c and d show that the threshold voltage is mainly dependent on the distance between the tip position and the nearest grain boundary. Fig. 2e shows the threshold voltage as a function of the distance obtained from measurements at various locations and a lot of grains. We can clearly see that the farther the tip contacts location away from the nearest grain boundary, the larger the threshold voltage is.

Usually, the maximum practical capacity of $LiCoO_2$ material is only half of the theoretical value while working under a cutoff voltage (*e.g.* 4.2 V with Li metal as the anode). A larger charge voltage can provide a higher capacity, but easily destroy the $LiCoO_2$ lattice structures and result in a rapid capacity loss[24]. Therefore, LIBs with a high capacity and optimized charge voltage are desired. As shown in Fig. 2e, if we take 2.5 V as a constant bias voltage, a high capacity density is expected to be achieved in a Li_xCoO_2 electrode with a grain
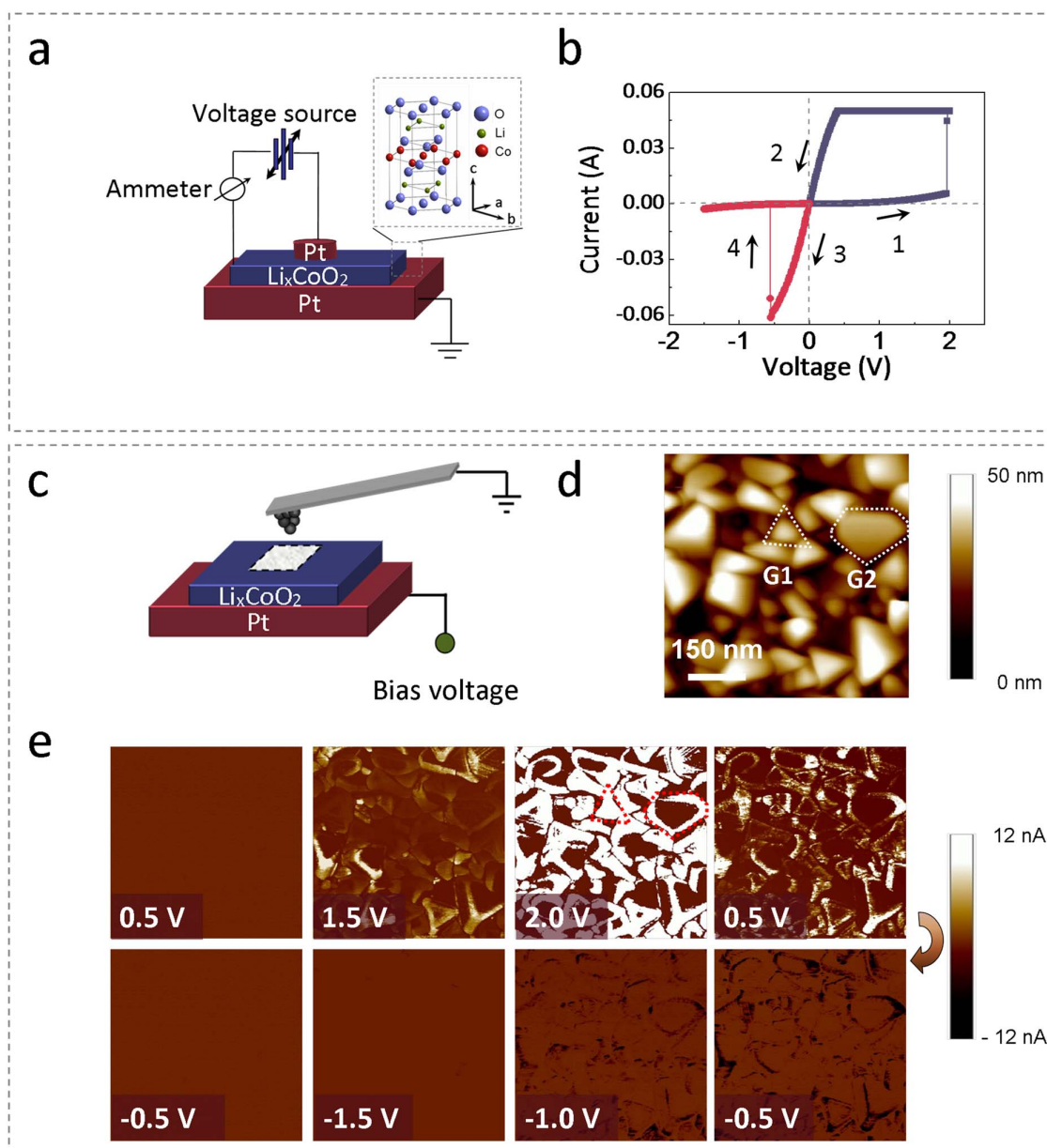
Figure 1 | Characterization of conductance change behaviors in Li_xCoO_2 films under various electrical fields. (a) Schematic of a sandwiched Pt/Li_xCoO_2/Pt structure. (b) Typical *I–V* characteristics observed in the Pt/Li_xCoO_2/Pt device. (c) Schematic of C-AFM measurements on Li_xCoO_2 films. (d,e) Morphology of a Li_xCoO_2 thin film (d), and current images scanned at various bias voltages (e). The dashed boxes mark two grains (G1 and G2, respectively) in Fig. 1d and their current images under a bias voltage of 2 V in Fig. 1e.

size less than about 50 nm (with a distance range of around 25 nm), in which a certain amount of Li ions in the whole grain can be de-intercalated. In order to verify this speculation, we chose a Li_xCoO_2 grain with a lateral size of around 45 nm and studied the local conductance of the grain after applying various bias voltages. After each scanning process, the grain conductance mapping was recorded at 0.5 V (Fig. 3a), followed by negative bias scanning processes similar to the procedures performed in Fig. 1e (This also demonstrated that the Li-ion can be reversibly intercalated/de-intercalated in the grain and the $LiCoO_2$ structure is stable). As expected, more and more well conductive areas indicate the Li-deficient area extended from grain boundaries to grain interiors with increased bias voltage. After a 2.5 V scanning process, both boundary area and interior reached the compliance current level ($\sim$12 nA), implying that a certain amount of Li ions have been uniformly de-intercalated. We noted that at high conductive states, the currents were usually proportional to the bias voltages, following ohm's law (also see Fig. 2b). As a result, the conductance values can be obtained by simply using $G=I/V$. Fig. 3b shows the location dependence of normalized conductivity after various bias voltage scanning processes in the grain (see Definition of normalized conductivity in Methods). Fig. S5 in supplementary show the resistive/conductivity and corresponding normalized conductivity of Li_xCoO_2 bulk samples as a function of Li content[25]. If we coarsely assume that the compliance current level ($\sim$12 nA) corresponds to the current of the Li-deficient Li_xCoO_2 detected at 0.5 V, in which a certain amount of Li ions have been extracted (in a extreme condition, i.e. x=0), we may evaluate roughly Li distributions in the grain at different locations (Fig. 3b). For comparison, we also studied the location dependence of normalized conductivity in a larger grain ($\sim$120 nm) following the same measuring procedures. It was found that the grain interiors were always much more insulating than grain boundary areas, even after a 2.5 V scan-
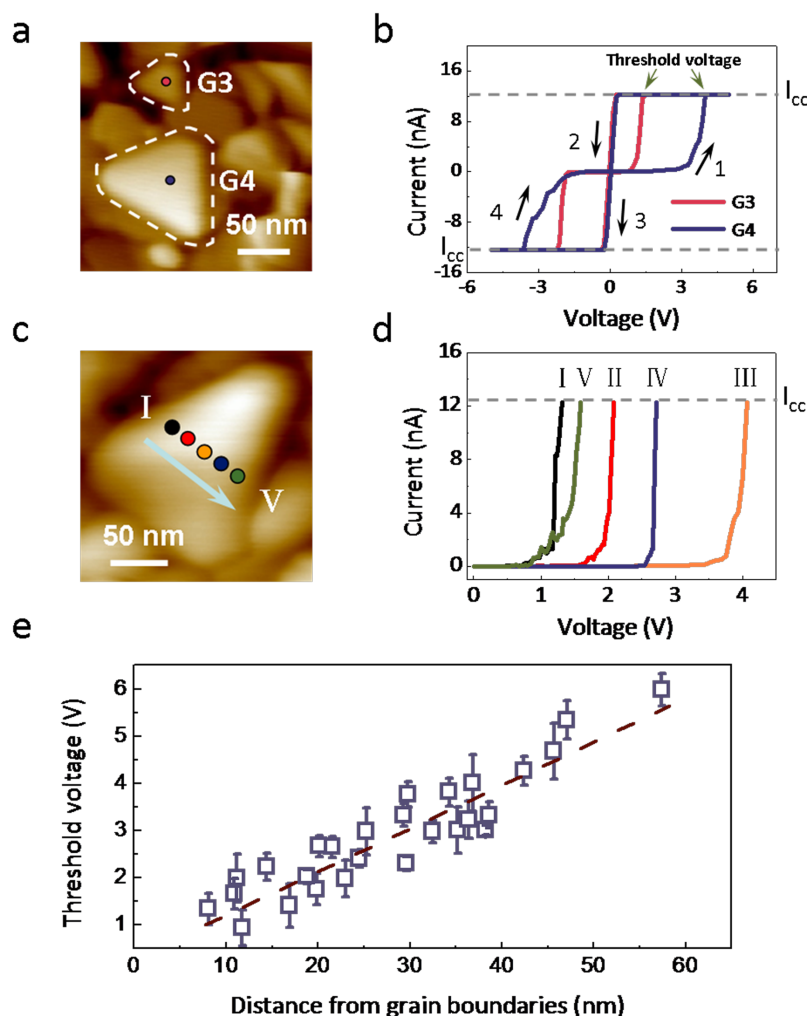
Figure 2 | Characterization of Li-ion de-intercalation threshold voltages in Li$_x$CoO$_2$ grains by using C-AFM tip measurement *in situ*. (a,b) Morphology of a selected area on a Li$_x$CoO$_2$ film (a) and corresponding *I–V* curves (b) showing different conductance change behaviors of two grains, G3 and G4, respectively. The C-AFM tip locations were marked at the spots in Fig. 2a. (c,d) Morphology of a Li$_x$CoO$_2$ grain (c) and corresponding *I–V* curves (d) at different positions away from grain boundaries in the same grain. The C-AFM tip locations were marked at the spots from I to V in Fig. 2c. (e) Location dependence of the threshold voltage obtained from various grains. The threshold voltage is defined as the critical voltage where the grain is switched to a conductive state (see Fig. 2b), and the distance is the shortest distance between the tip location and the nearest grain boundary. The line is a guide to the eye.

ning process (Fig. 3c). In other words, from the point view of Li-ion diffusion behaviors, under a certain bias voltage, more Li ions can be extracted from the Li$_x$CoO$_2$ nanograins with a smaller grain size in a given time. As a result, one can achieve LIBs with a high capacity by using small LiCoO$_2$ nanograins as cathode and charging under a suitable bias voltage.

To understand the experimental observations aforementioned, we performed first principles calculation. Perfect LiCoO$_2$ crystal is composed of CoO$_2$ sheets stacked in the [001] direction with Li layers intercalated in between. Each CoO$_2$ sheet is built from units of edge-sharing CoO$_6$ octahedrons, which form an extensive two-dimensional network parallel to the (001) plane. These edge-sharing CoO$_6$ octahedrons are packed very close to each other (see Fig. S6). Our calculation results show that the Li-ion diffusion energy barrier along a vertical direction directly through the CoO$_2$ sheet is around 6.8 eV. However, the Li-ion diffusion energy barrier along CoO$_2$ sheets is only 0.3 eV (well consistent with ref. 34). In practical LIBs, under a bias voltage, Li-ion will first diffuse along CoO$_2$ sheets and then transfer along grain boundaries[14,35]. To model the grain boundaries, different low-index crystal planes {100}s and {110}s which are parallel to the [001] direction were considered. The grain

boundary structure can be understood as a stacking fault with a relative displacement of a 1/2 unit cell along the [001] direction and a schematic of the (100) grain boundary was shown in Fig. 4a. Our calculation results show that both (100) and (110) grain boundaries are very stable with very low formation energy of 0.08 eV/Å^2 and 0.05 eV/Å^2, respectively. As a result of the relative displacement, Li layers, which are originally separated by close-packed CoO$_6$ octahedrons layers, are now only separated by O layers (Fig. 4a), and periodic gaps are created in the network of CoO$_2$ sheets at grain boundaries (Fig. 4b,c). Therefore, Li ions at grain boundaries are now connected by a clear and continuous diffusion channel along the [001] direction, providing a 0.7 eV diffusion energy barrier pathway along the [001] direction, which is a steep decline from 6.8 eV for the Li-ion to cross the CoO$_2$ sheet. This is in good agreement with our experimental results that the Li-ion diffusion energy barrier is much lower near grain boundaries than that at grain interiors.

Discussion

Since we have clarified the correlation between the capacity density (indicated by the high conductive area density) and grain boundary area (grain size) of Li$_x$CoO$_2$ nanograins, then we further
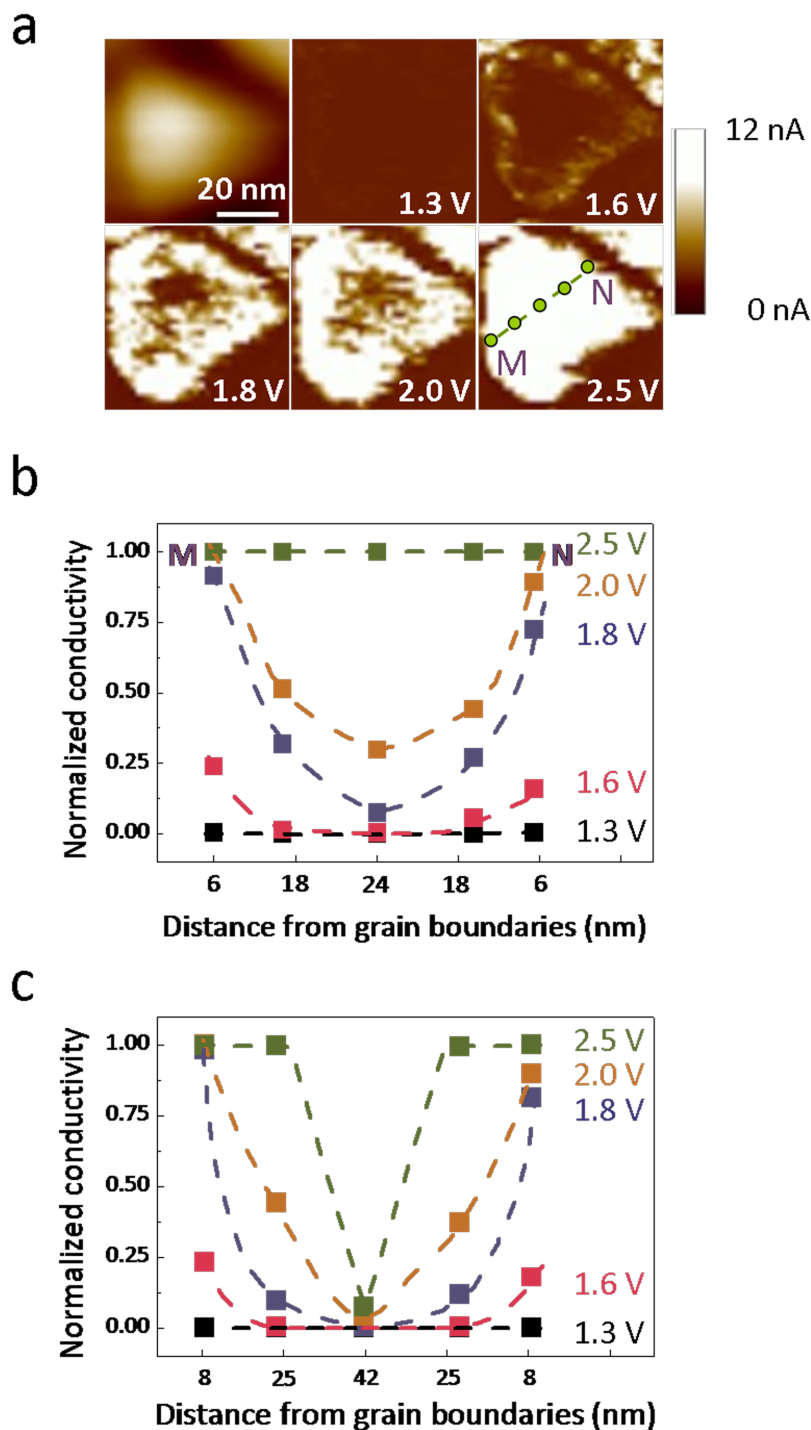
Figure 3 | Characterization of local normalized conductivity in Li_xCoO_2 grains after applying various bias voltages. (a) Morphology image and current images obtained at 0.5 V after scanning the sample under various bias voltages. The amplitude of the voltages applied to change the conductance states before C-AFM acquirements are shown in the corresponding current images. (b) Normalized conductivity as a function of the distance away from the nearest grain boundary. The specific tip locations are indicated in the current image in Fig. 3a. The lateral size of the scanned grain is around 45 nm. (c) Normalized conductivity as a function of the distance away from the nearest grain boundary in a larger grain (~120 nm) after applying various bias voltage scanning processes. All lines are guides to the eye.

characterized the high-rate charge characteristics by studying the kinetics of Li-ion diffusion in the Li_xCoO_2 nanograins. With locating tip at different locations on a grain and applying a constant bias voltage, the corresponding current-time characteristics were investigated. It is found that the current increasing rates near boundaries, where the energy barrier is relatively lower, are higher than that at interiors (see Fig. S7). This suggests that LIBs with good high-rate capability may be realized by adapting Li_xCoO_2 electrodes composed

of nanograins with a large grain boundary area. However, more reliable data about the Li-ion diffusion kinetics information is unavailable at this stage, due to sample thermal drift with increased data acquisition time during the measurements and some other technical problems[14].

As aforementioned, we mainly studied the diffusion behaviors of Li-ion out of the Li_xCoO_2 nanograins under bias voltages. The diffusion behaviors of Li-ion back to the nanograins also need to be
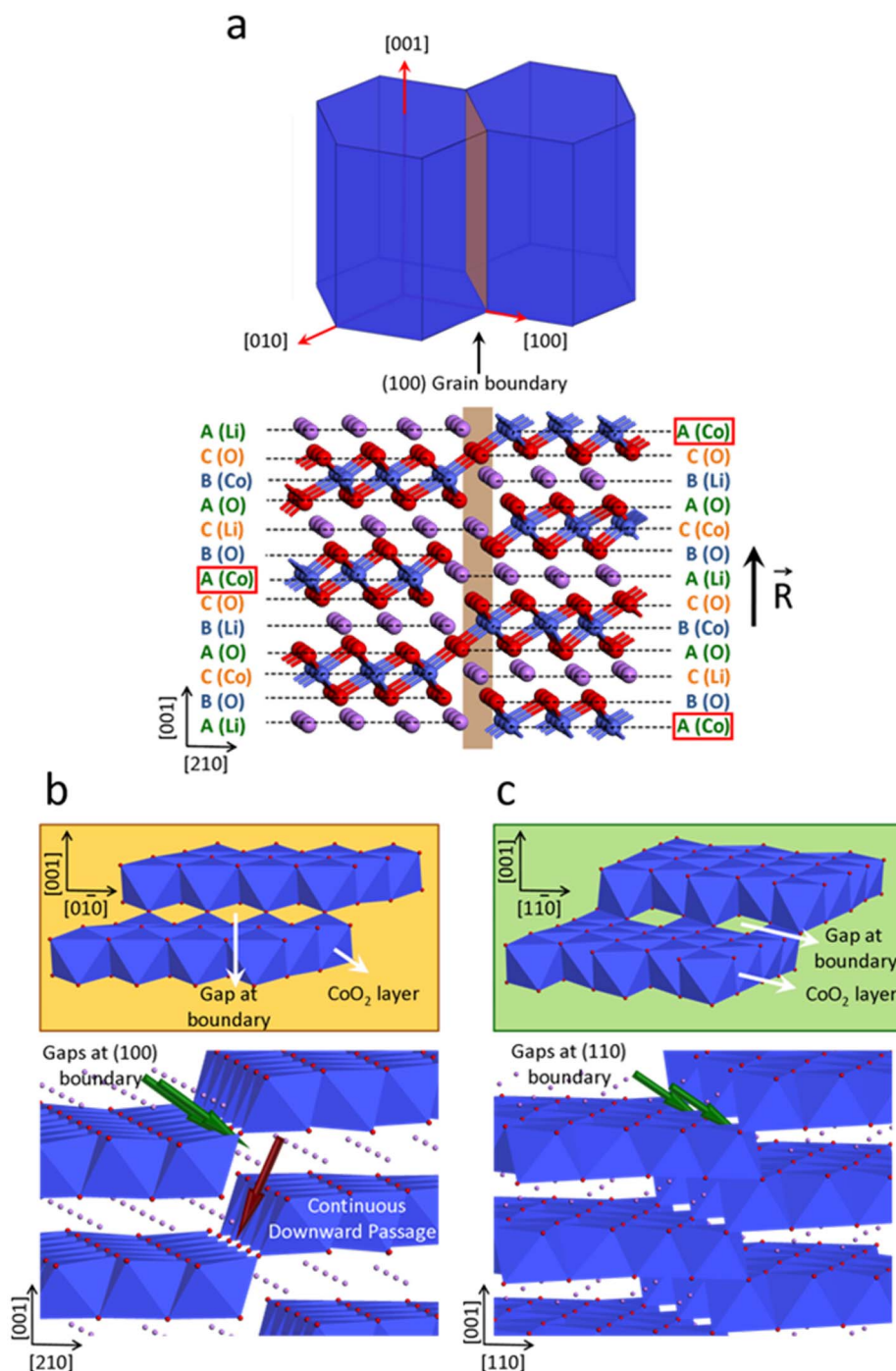
Figure 4 | Models of Li-ion transport along grain boundaries. (a) Schematic illustration of the grain boundary along (100) plane. (b,c) Schematic illustrations of Li-ion diffusion paths along (100) (b) and (110) (c) grain boundaries.

addressed. In fact, the diffusion of Li-ion back to the interiors has been demonstrated by Balke *et al* using electrochemical strain microscopy to detect topographic changes[14]. In our case, the movement of Li-ion back to the nanograins under negative bias voltages can be expected based on the observation of insulating/semiconductive behaviors of the nanograins (Fig. 1e) and the Pt/Li_xCoO_2/Pt device after being switched back to the low conductive state (Fig. S2). From Fig. 2b, one can see that the threshold voltages for the transitions between the high and low conductive states at the same location are nearly the same, which indicates that the diffusion of Li-ion back to the grain interiors also requires a larger bias voltage in contrast with grain boundaries.

In summary, we successfully mapped the Li-ion transport behaviors in Li_xCoO_2 nanograins under an electrical field by using C-AFM technique to study the local conductance variations with a spatial resolution of ~10 nm. It was found that the area near grain boundaries can easily become more conductive in contrast with grain interiors under a certain bias voltage. This is consistent with our first principles calculation, which shows that grain boundary has a very low Li-ion diffusion energy barrier. This finding along with the studies of local conductance characteristics which reveal the local Li distributions and Li-ion diffusion kinetics in Li_xCoO_2 nanograins under electrical fields suggest that high-rate charge LIBs with a high capacity can be achieved by adapting Li_xCoO_2 nanostructured

electrodes composed of grains with a large grain boundary area and using a suitable charge voltage. This information offers important guidelines for LIBs engineering from a point view of optimizing the electrode material microstructures. Moreover, the investigation of ion transportation in combination with conductance change characteristics by using C-AFM technique at a nano-scale will benefit the development of ionic memories and nanoionics.

Methods

Sample preparation. For the $Pt/Li_xCoO_2/Pt$ devices, the Pt top electrodes with a diameter of 100 μm and a thickness of 80 nm were deposited by using e-beam evaporation with a metal shadow mask *in situ*.

Measurements. The crystal structure was examined by using XRD (Huber six-circle diffractometer). The conductance change behaviors and temperature dependence of resistances at low and high conductive states for the $Pt/Li_xCoO_2/Pt$ devices were characterized using a Keithley 4200 semiconductor parameter analyzer. The I–V sweep rate is around 0.25 V/s. The conductance values of different conductive states are obtained under a reading voltage of 0.1 V. An atomic force microscopy (Dimension V, Veeco) equipped with a conducting cantilever coated with Pt/Ir was employed for C-AFM measurements and contact mode was selected. The contact force between the tip and the sample is around 30 nN. During the measurement, the tip was grounded while a bias voltage was applied on the Pt substrate. The time of each pixel takes in current images during scanning process is around 2 ms. During the local I–V measurements the scan rate is set to 1 Hz. In order to get more reliable results, we chose relatively flat grains in this work to minimize the effect of topography. The sample drift was adjusted by offsetting the scanning area each time with some featured nanograins as a landmark.

Definition of normalized conductivity. For materials following ohm's law, the conductance can be defined as $G=I/V$, and the conductivity is defined as $\sigma=J/E$, where J is the current density and E represents the electrical field. For a uniform material with a regular shape, the conductance equals to the product of the material conductivity and a coefficient, which dependents on the length and cross-sectional area of the material. In our case, the tip contact area and the grain thickness for a flat Li_xCoO_2 grain are generally fixed, so the ratio of the conductance variations can reflect the conductivity changes. Thus, the normalized conductance equals to the normalized conductivity in value. As indicated in Fig. 1 and 2, a bias voltage of 0.5 V doesn't change the local conductance, so the conductance values can be calculated at 0.5 V. Thus, the normalized conductivity shown in Fig. 3 corresponds to the normalized conductance at 0.5 V.

First principles calculation and modeling. To model the $LiCoO_2$ grain boundary, we carry out first principles calculation based on the Density Functional Theory (DFT) as implemented in the Vienna ab-initio simulation package (VASP). Exchange and correlation effects were incorporated within the generalized gradient approximation (GGA), using the Perdew-Wang 91 (PW91) functional[36]. Vosko-Wilk-Nusair interpolation[37] was used for the correlation part of the exchange correlation functional. Interaction between ions and electrons was described using the projector augmented wave method[38]. Cutoff energy was set at 400 eV for the plane-wave basis. In all calculations, self-consistency was achieved with accuracy of at least 10^{-3} and 10^{-4} eV for the ionic and electronic loops respectively. All k points were generated using G-centered grids based on the Monkhorst-Pack scheme[39]. The geometry of each periodic supercell has been optimized based on the perfect supercell. For $LiCoO_2$, the computed lattice parameters of a = b = 2.85 Å, c = 14.05 Å, which is in very good agreement with experimental results where a = b = 2.81 Å, c = 14.04 Å[40].

The grain boundary was modeled using a periodic supercell consisting of two such boundaries along the same plane. The (100) boundary was modeled with a 5.71 Å × 9.89 Å × 14.05 Å supercell and the k points were generated with a 4 × 3 × 2 grid. The (110) boundary was modeled with a 4.94 Å × 11.42 Å × 14.05 Å supercell and the k points were generated with a 5 × 2 × 2 grid. The formation energy of two-dimensional (2D) grain boundaries was calculated by using: $E_F = 1/2(E - E_{bulk})/A$, where E is the total energy of the supercell containing two such boundaries, E_{bulk} is the total energy of the corresponding perfect supercell with no boundaries and A is the cross-sectional area of the boundary. For the (100) boundary, the two boundaries in a supercell are not identical and the formation energy reported is the mean of these two.

1. Maier, J. Nanoionics: ion transport and electrochemical storage in confined systems. *Nat. Mater.* **4**, 805–815 (2005).
2. Maier, J. Nano-Ionics: More Than Just a Fashionable Slogan. *J. Electroceram.* **13**, 593–598 (2004).
3. Armand, M. & Tarascon, J. M. Building better batteries. *Nature* **451**, 652–657 (2008).
4. Waser, R. & Aono, M. "Nanoionics-based resistive switching memories." *Nat. Mater.* **6**, 833–840 (2007).
5. Lu, W., Jeong, D. S., Kozicki, M. & Waser, R. Electrochemical metallization cells—blending nanoionics into nanoelectronics? *MRS Bull.* **37**, 124 (2012).
6. Simon, P. & Gogotsi, Y. Materials for electrochemical capacitors. *Nat. Mater.* **7**, 845–854 (2008).
7. Tarascon, J. M. & Armand, M. Issues and challenges facing rechargeable lithium batteries. *Nature* **414**, 359–367 (2001).
8. Guo, Y. G., Hu, J. S. & Wan, L. J. Nanostructured Materials for Electrochemical Energy Conversion and Storage Devices. *Adv. Mater.* **20**, 2878–2887 (2008).
9. Wang, Y. & Cao, G. Developments in Nanostructured Cathode Materials for High-Performance Lithium-Ion Batteries. *Adv. Mater.* **20**, 2251–2269 (2008).
10. Kalinin, S. V. & Balke, N. Local Electrochemical Functionality in Energy Storage Materials and Devices by Scanning Probe Microscopies: Status and Perspectives. *Adv. Mater.* **22**, E193–E209 (2010).
11. Malik, R., Zhou, F. & Ceder, G. Kinetics of non-equilibrium lithium incorporation in $LiFePO_4$. *Nat. Mater.* **10**, 587–590 (2011).
12. Van der Ven, A., Bhattacharya, J. & Belak, A. A. Understanding Li Diffusion in Li-Intercalation Compounds. *Acc. Chem. Res.* (2012) DOI: 10.1021/ar200329r.
13. Orsini, F. *et al. In Situ* Scanning Electron Microscopy (SEM) observation of interfaces within plastic lithium batteries. *J. Power Sources* **76**, 19–29 (1998).
14. Balke, N. *et al.* Nanoscale mapping of ion diffusion in a lithium-ion battery cathode. *Nat. Nanotech.* **5**, 749–754 (2010).
15. Lipson, A. L., Ginder, R. S. & Hersam, M. C. Nanoscale *In Situ* Characterization of Li-ion Battery Electrochemistry Via Scanning Ion Conductance Microscopy. *Adv. Mater.* **23**, 5613–5617 (2011).
16. Bhattacharyya, R. *et al.* In situ NMR observation of the formation of metallic lithium microstructures in lithium batteries. *Nat. Mater.* **9**, 504–510 (2010).
17. Chandrashekar, S. *et al.* ^{7}Li MRI of Li batteries reveals location of microstructural lithium. *Nat. Mater.* **11**, 311–315 (2012).
18. Shao-Horn, Y., Croguennec, L., Delmas, C., Nelson, E. C. & O'Keefe, M. A. Atomic resolution of lithium ions in $LiCoO_2$. *Nat. Mater.* **2**, 464–467 (2003).
19. Choi, S. H., Kim, J. & Yoon, Y. S. A TEM study of cycled nano-crystalline HT-LiCoO2 cathodes for rechargeable lithium batteries. *J. Power Sources* **135**, 286 (2004).
20. Huang, J. Y. *et al.* In Situ Observation of the Electrochemical Lithiation of a Single SnO2 Nanowire Electrode. *Science* **330**, 1515 (2010).
21. Chan, C. K. *et al.* High-performance lithium battery anodes using silicon nanowires. *Nat. Nanotech.* **3**, 31 (2008).
22. Wang, C.-M. *et al.* In Situ TEM Investigation of Congruent Phase Transition and Structural Evolution of Nanostructured Silicon/Carbon Anode for Lithium Ion Batteries. *Nano Lett.* **12**, 1624 (2012).
23. Liu, X. H. & Huang, J. Y. In situ TEM electrochemistry of anode materials in lithium ion batteries. *Energy Environ. Sci.* **4**, 3844 (2011).
24. Xia, H., Lu, L., Meng, Y. S. & Ceder, G. Phase transitions and high-voltage electrochemical behavior of $LiCoO_2$ thin films grown by pulsed laser deposition. *J. Electrochem. Soc.* **154**, A337–A342 (2007).
25. Motohashi, T. *et al.* Impact of lithium composition on the thermoelectric properties of the layered cobalt oxide system Li_xCoO_2. *Phys. Rev. B* **83**, 195128 (2011).
26. Chen, A. Ionic Memory Technology. Solid State Electrochemistry II, Wiley-VCH Verlag GmbH & Co. KGaA: 1–30 (2011).
27. Moradpour, A. *et al.* Resistive Switching Phenomena in Li_xCoO_2 Thin Films. *Adv. Mater.* **23**, 4141–4145 (2011).
28. Ohnishi, T., Hang, B. T., Xu, X., Osada, M. & Takada, K. Quality control of epitaxial $LiCoO_2$ thin films grown by pulsed laser deposition. *J. Mater. Res.* **25**, 1886–1889 (2011).
29. Bates, J. B. *et al.* Preferred Orientation of Polycrystalline $LiCoO_2$ Films. *J. Electrochem. Soc.* **147**, 59–70 (2000).
30. Kwon, D.-H. *et al.* Atomic structure of conducting nanofilaments in TiO_2 resistive switching memory. *Nat. Nanotech.* **5**, 148 (2010).
31. Russo, U., Ielmini, D., Cagli, C. & Lacaita, A. L. Self-Accelerated Thermal Dissolution Model for Reset Programming in Unipolar Resistive-Switching Memory (RRAM) Devices. *IEEE Tran. Electr. Dev.* **56**, 193 (2009).
32. Yang, Y. C., Pan, F. & Zeng, F. Bipolar resistance switching in high-performance Cu/ZnO:Mn/Pt nonvolatile memories: active region and influence of Joule heating. *NEW J. PHYS.* **12**, 023008 (2010).
33. Bruce, G. P. Solid-state chemistry of lithium power sources. *Chem. Commun.* 1817–1824 (1997).
34. Van der Ven, A. & Ceder, G. Lithium diffusion mechanisms in layered intercalation compounds. *J. Power Sources* **97**, 529–531 (2001).
35. Park, M., Zhang, X., Chung, M., Less, G. B. & Sastry, A. M. A review of conduction phenomena in Li-ion batteries. *J. Power Sources* **195**, 7904–7929 (2010).
36. Wang, Y. & Perdew, J. P. Correlation hole of the spin-polarized electron gas, with exact small-wave-vector and high-density scaling. *Phys. Rev. B* **44**, 13298–13307 (1991).
37. Vosko, S. H., Wilk, L. & Nusair, M. Accurate spin-dependent electron liquid correlation energies for local spin density calculations: a critical analysis. *Can. J. Phys.* **58**, 1200–1211 (1980).

38. Kresse, G. & Joubert, D. From ultrasoft pseudopotentials to the projector augmented-wave method. *Phys. Rev. B* **59**, 1758–1775 (1999).

39. Monkhorst, H. J. & Pack, J. D. Special points for Brillouin-zone integrations. *Phys. Rev. B* **13**, 5188–5192 (1976).

40. Ohzuku, T., Ueda, A., Nagayama, M., Iwakoshi, Y. & Komori, H. Comparative study of $LiCoO_2$, $LiNi_{12}Co_{12}O_2$ and $LiNiO_2$ for 4 volt secondary lithium cells. *Electrochim. Acta* **38**, 1159–1167 (1993).

Acknowledgements

Author contributions

R.-W.L. and J.D. conceived and designed the experiments. X.X. fabricated the Li_xCoO_2 samples. X.Z. carried out the experiments and corresponding results analysis. J.D. and C.O. developed the model and performed 1st principles calculation. X.Z., J.D., C.O., X.X. and R.-W.L. co-wrote the paper. All authors commented on the manuscript.

Additional information

Supplementary information accompanies this paper at http://www.nature.com/scientificreports

Competing financial interests: The authors declare no competing financial interests.

How to cite this article: Zhu, X. *et al.* Direct observation of lithium-ion transport under an electrical field in Li_xCoO_2 nanograins. *Sci. Rep.* **3**, 1084; DOI:10.1038/srep01084 (2013).